

Correlations versus noise in the NFT market

Marcin Wątopek,¹ Paweł Szydło,¹ Jarosław Kwapien,² and Stanisław Drożdż^{1,2}

¹*Faculty of Computer Science and Telecommunications, Cracow University of Technology, ul. Warszawska 24, 31-155 Kraków, Poland*

²*Complex Systems Theory Department, Institute of Nuclear Physics, Polish Academy of Sciences, ul. Radzikowskiego 152, 31-342 Kraków, Poland*

(*Electronic mail: marcin.watorek@pk.edu.pl)

(Dated: 25 April 2024)

The non-fungible token (NFT) market emerges as a recent trading innovation leveraging blockchain technology, mirroring the dynamics of the cryptocurrency market. To deepen the understanding of the dynamics of this market, in the current study, based on the capitalization changes and transaction volumes across a large number of token collections on the Ethereum platform, the degree of correlation in this market is examined by using the multivariate formalism of detrended correlation coefficient and correlation matrix. It appears that correlation strength is lower here than that observed in previously studied markets. Consequently, the eigenvalue spectra of the correlation matrix more closely follow the Marchenko-Pastur distribution, still, some departures indicating the existence of correlations remain. The comparison of results obtained from the correlation matrix built from the Pearson coefficients and, independently, from the detrended cross-correlation coefficients suggests that the global correlations in the NFT market arise from higher frequency fluctuations. Corresponding minimal spanning trees (MSTs) for capitalization variability exhibit a scale-free character while, for the number of transactions, they are somewhat more decentralized.

The complexity of financial markets, encompassing traditional assets and emerging forms like cryptocurrencies and non-fungible tokens (NFTs), is a multi-scale phenomenon driven by various factors. Understanding this complexity and the associated emergent phenomena requires delving into the details and intricacies of these markets, dynamic interaction of diverse elements, and the evolving system of global finance. NFTs represent a unique form of digital assets, often tied to digital art, collectibles, or virtual real estate. The subtleties related to complexity of NFT markets arise from their innovative nature resulting from the valuation of digital assets, intellectual property considerations, and the variety of smart contracts. NFTs also introduce new possibilities for creators and collectors, but come with challenges related to copyright, authenticity, and market saturation. The issue of global correlations within NFT markets has not been quantitatively addressed in the literature so far and therefore, in this study, it is framed in the context of the potential competition between correlation effects and randomness.

creation of one's own fungible tokens in ERC-20 standard⁴. One of the applications of smart contracts was one of the first and highest-valued NFT collections - CryptoPunks, even though the concept of unique tokens is older and can be traced back to 2012 Bitcoin colored coins⁵ and the creation of the first-ever NFT, Quantum, minted by Kevin McCoy on Namecoin in 2014⁶. The Ethereum project experienced significant growth and development, particularly in 2017, when numerous projects launched on its blockchain through initial coin offerings (ICOs), ultimately contributing to a market bubble⁷. At the peak of the ICO bubble in December 2017, the challenges in the capacity of the Ethereum network became increasingly evident. The surge in popularity of the CryptoKitties game exacerbated these issues, at times consuming up to 70% of Ethereum's usage capacity. This spike in demand led to record highs in the number of transactions and fees, considerably slowing down the network⁸. The game enables participants to purchase, sell, and create non-fungible tokens (NFTs) on the Ethereum blockchain. It stands out as one of the earliest and most prominent examples of the ERC-721 standard, which became officially recognized as the Non-Fungible Token standard in 2018⁹. This standard facilitates the straightforward creation of NFT tokens and collections by anyone.

I. INTRODUCTION

The cryptoassets space is constantly evolving. Since the first cryptocurrency - Bitcoin - launched in 2009¹, blockchain technology has undergone considerable evolution and found applications in various fields². The initial functionality of Bitcoin and its early alternatives was limited to settling transactions and serving as a distributed ledger register. This changed with the launch of Ethereum in 2015 as a decentralized, open-source, and distributed computing platform³. This marked the first significant expansion of blockchain capabilities. The Ethereum smart contracts functionality allowed for the easy

The application of smart contracts to finance marked a significant second milestone for the cryptoasset domain, giving rise to the phenomenon known as DeFi (Decentralized Finance) Summer that lasted between mid-2020 and early 2021¹⁰. This was accompanied by the development of blockchains that competed with Ethereum, such as Solana, Avalanche, Arbitrum, BNB Chain, Polygon, Tron, Optimism, and Cardano. The total value locked in DeFi protocols on various blockchains peaked in Dec 2021 with a value of 250 billion USD¹¹. In this period, NFT tokens surged in popularity and entered the mainstream, driven by a low barrier to entry, the simplicity of launching personal collections, and celebrity endorsements. These factors fueled the speculative NFT bub-

ble of 2021¹². The boom started in March 2021 when Mike Winkelmann, aka Beeple, sold his NFT *Everydays: The First 5,000 Days* (2021) for \$69 million at Christie's¹³. Shortly after that, the 10,000-part series *Bored Ape Yacht Club* was launched in May 2021, starting a wave of similar projects called profile-pic NFTs (PPF NFTs). Many celebrities owed a Bored Ape Yacht Club NFT or released their own collections^{14–16} and even the former US president Donald Trump had participated in the NFT collective enthusiasm¹⁷. After spectacular growth, when the most expensive NFT token (CryptoPunk #5822) was sold for 8000 ETH in February 2022, the NFT market eventually peaked in May 2022, reaching a total capitalization of ~ 21 billion USD¹⁸. The widespread popularity of NFTs at that time allowed for funding support for Ukraine via selling one of the CryptoPunk tokens in June 2022 for 90 ETH ($\sim 100,000$ USD). After the subsequent crash¹⁹, the total capitalization dropped to 5 billion USD in April 2024²⁰. Given the unregulated nature of the NFT market, it has been subject to numerous manipulative practices^{21,22} including wash trading²³ and pump-and-dump schemes²⁴.

Despite a dramatic drop of nearly 90% in market value, the blockchain technology underpinning NFTs continues to evolve. The Bitcoin Ordinals protocol was introduced to the Bitcoin network in January 2023²⁵, enabling the creation of collections on the Bitcoin blockchain. In December 2023, this blockchain accounted for the largest portion of NFT trading volume at 42.1%. Nonetheless, throughout 2023, Ethereum maintained its position as the dominant blockchain for NFT transactions with 72.3% trading volume share²⁶. Other blockchains hosting NFT collections include Solana, Immutable X, Polygon, BNB Chain, Flow, Arbitrum, Avalanche, and Ronin. There are many NFT marketplaces that enable NFT collections trading; the three largest ones are Blur, Magic Eaden and OpenSea as of April 2024²⁷. Although the current main NFT application to pure speculation faced serious criticism²⁸ and, despite many challenges²⁹, the standard may still represent a paradigm shift in how digital assets are perceived, owned, and transacted, reshaping the digital world's understanding of value and ownership^{30,31}.

Building on our previous exploration of price fluctuation characteristics within individual NFT collections³², this article aims to delve into the correlations among NFT collection trades. The well-established financial markets, such as stocks^{33,34}, Forex^{35–37}, and even younger cryptocurrencies^{38–45}, demonstrate significant collective behavior in their cross-correlations. Random Matrix Theory (RMT) has been effectively utilized to uncover the nature and origins of correlations in these markets^{46–48}. In this study, RMT is applied to examine the price and the number of transactions variations of the collections created on the Ethereum blockchain. This analysis will focus on determining the non-random nature of these correlations and examining if distinct NFT-market sectors can be distinguished. Properties of minimal spanning trees constructed from the correlation networks based on correlation matrices will also be analyzed. This approach has already been successfully applied to financial time series^{49,50}, including stocks^{51–53}, currencies^{36,54}, and cryptocurrencies^{41,55–58}.

II. DATA AND METHODS

A. Data specification

The dataset contains tick-by-tick data representing transactions (price and time) on 90 NFT collections from the Ethereum blockchain. It covers the period of $T = 500$ days that began on June 9, 2022 and ended on October 21, 2023. The data was sourced from the CryptoSlam! portal⁵⁹. The collections were selected according to the criterion requiring that, on average, each collection had at least two transactions involving at least one of its tokens. Each dataset was then converted into a bivariate time series representing (1) the collection capitalization logarithmic increments $c_{\Delta t}(t) = \ln K(t + \Delta t) - \ln K(t)$ expressed in USD, where $K(t)$ is the total capitalization at a moment t , and (2) the number $N_{\Delta t}$ of transactions in time unit Δt . Two sampling frequencies were chosen: $\Delta t = 1h$, suitable for the 13 most liquid collections where less than 50% of hours had no trading activity (see the column $\%0_{\Delta t=1h}$ in Tab. I), and $\Delta t = 24h$, applicable to all collections. Transaction prices in various cryptocurrencies were also available for extraction. However, since transactions on the Ethereum blockchain occur not only in ETH but also in a multitude of other tokens, this information proved to be impractical for consolidation into a single time series. The complete list of the collections, along with their basic characteristics such as capitalization on the dataset's final day, the total number of transactions, collection size measured by the number of circulated tokens, and a fraction of the hours without transactions, can be found in Tab. I.

Capitalization $K(t)$ and the number of transactions $N_{\Delta t=24h}(t)$ for all the collections are depicted in Fig. 1(a)(b). As shown in panel (a), most collections experienced a decrease in $K(t)$ during the studied period, reflecting the overall downtrend in the NFT market. An exception to this trend is Milady Maker collection, which experienced significant capitalization gains in April and May 2023. These gains were accompanied by a surge in transaction activity, with the collection recording the highest daily transaction count among all collections in the period studied, reaching approximately 1,600 transactions on May 10, 2023. The unique trend observed in Milady Maker NFTs can be attributed to Elon Musk's tweet about this collection on this specific day and to the subsequent price rally⁶⁰. Other collections with a lower capitalization that experienced slight valuation increases include Lil Pudgys, Sappy Seals, and Pudgy Penguins. These collections also rank among the most frequently traded ones, although the general rule is that the most capitalized collections tend to be traded more frequently. The only exception is CryptoPunks, which despite the largest capitalization, have seen fewer transactions recently, likely due to their long-standing presence in the market. Another interesting spike in activity was observed on January 6, 2023 among less frequently traded and lower-capitalized collections such as Alien Frens, Killer GFs, Rug Radio - Genesis, Karafuru, Coolman's Universe, 3Landers, and Goblintown. On that date, these collections experienced a significantly higher than average transaction volume and a notable drop in capitalization, as illus-

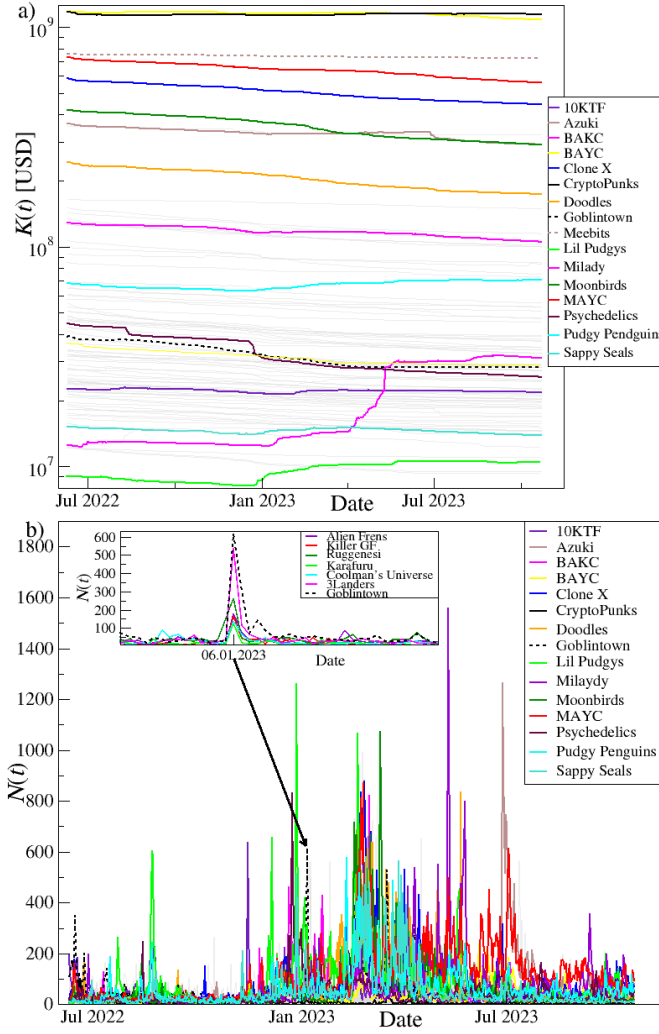


FIG. 1. (a) Collection capitalization $K(t)$ and (b) the number of transactions $N_{\Delta t=24h}(t)$ for all the considered NFT collections with the most frequently traded ones listed explicitly. Inset in (b) displays fluctuations of the number of transactions around January 6, 2023, highlighting a significant surge in activity for the aforementioned collections during this period.

trated in inset to Fig. 1(b).

Various patterns of activity in financial markets are observed^{61–63}, which can be linked to the start/end of trading sessions, specific days of the week, and macroeconomic news announcements. This patterned behavior is mirrored in the cryptocurrency market as well⁶⁴. Given this context, it became compelling to investigate the presence of similar trading activity patterns within the NFT market. By segmenting the number of transactions time series $N_{\Delta t=1h}$ into 500 time series for 24-hour-long periods and averaging across all trading days, a daily transaction pattern was identified - see Fig. 2. A period of the most frequent trading corresponds to the US day-time trading hours peaking around 12:00 UTC, which is 8:00 a.m. in New York. Most of the liquid collections see their highest activity levels during this window. Additionally, two other notable peaks occur at 16:00 and 18:00 UTC, when the

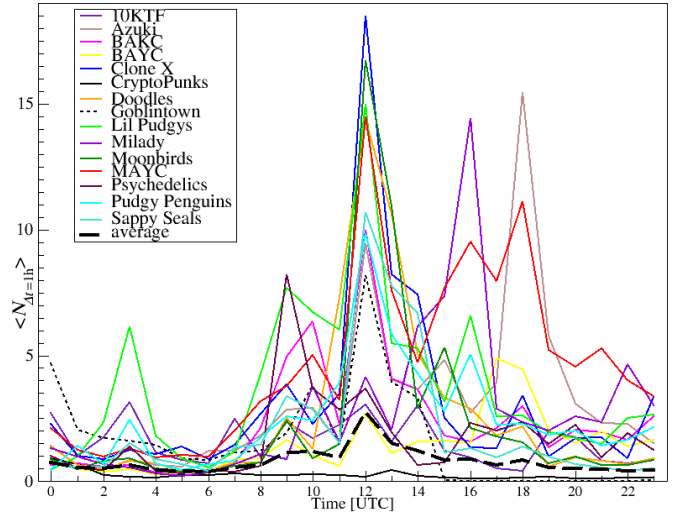


FIG. 2. Daily pattern of the number of transactions in 1 hour interval averaged over all trading days $\langle N_{\Delta t=1h} \rangle$.

most frequently traded collection - Monkey Ape Yacht Club - had the most transactions on average.

Understanding the characteristics of time series is crucial before proceeding with a correlation analysis, because this knowledge can help one in choosing the right correlation metrics. For this purpose, cumulative distributions of the capitalization increments $c_{\Delta t}$ and the number of transactions $N_{\Delta t}$ were analyzed for the 13 most liquid collections (those with $\%0_{\Delta t=1h} < 50\%$ in Table I). Fig. 3 shows that the cumulative probability distribution functions (CDFs) $P(X > \sigma)$, where σ denotes standard deviation, of $|c_{\Delta t}|$ and $N_{\Delta t}$ for all the collections exhibit heavy tails – a common characteristics of financial time series^{65–68}.

For the absolute capitalization increments $|c_{\Delta t}|$, the CDF tails follow a power law $x^{-\gamma}$ with the exponent γ varying between 1.5 and 2.0 for most collections – see Fig. 3(a). For the most liquid ones, such as Bored Ape Yacht Club and Mutant Ape Yacht Club, a stretched exponential function $\exp(x^\beta)$ provides a good fit if $\beta \approx 0.35$. In terms of the number of transactions $N_{\Delta t}$, the CDF tails are less heavy as compared to those for $|c_{\Delta t}|$, with the stretched exponential function accurately fitting the data for $0.3 \leq \beta \leq 0.4$. These findings align closely with the results from a previous study on the most liquid collections from the Solana blockchain³², where similar patterns were observed in the distributions of absolute capitalization increments and the number of transactions.

Another measure of temporal relationships in time series, which may involve both linear and non-linear dependencies, is the autocorrelation function

$$A(x, \Delta i) = \frac{1/T \sum_{i=1}^T [x(i) - \langle x(i) \rangle] [x(i + \Delta i) - \langle x(i) \rangle]}{\sigma_x^2}, \quad (1)$$

where σ_x^2 denotes variance of a time series $x(i)$, $\langle \cdot \rangle$ is mean, and Δi refers to a temporal lag measured in data points (which can be translated to time by $\tau = \Delta i \Delta t$). For the financial logarithmic returns, the autocorrelation function (ACF) shows

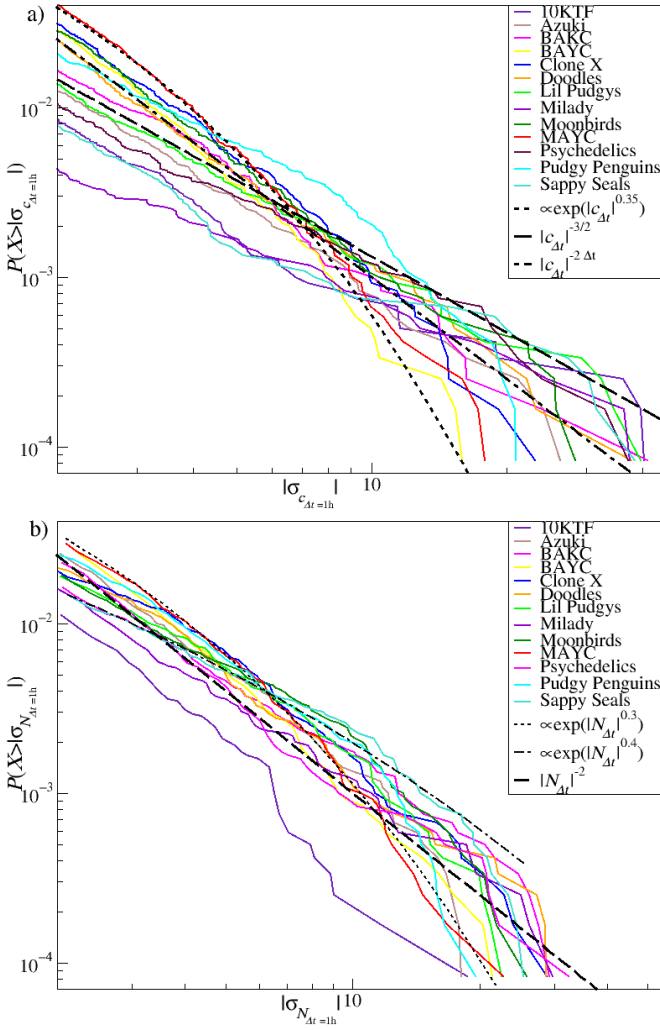


FIG. 3. Cumulative probability distribution functions for (a) absolute logarithmic increments of collection capitalization expressed in USD $|c_{\Delta t=1h}(t)|$ and (b) the number of transactions aggregated hourly $N_{\Delta t=1h}(t)$.

a characteristic behavior of dropping immediately to zero if their sign is taken into consideration and slowly decreasing according to a power law if their absolute values are considered⁶⁹. Fig. 4 presents ACFs for the 13 most liquid collections for both $|c_{\Delta t}|$ and $N_{\Delta t}$ with $\Delta t = 1h$. A consistent observation across these collections is a slow decay of $A(x, \tau)$ signaling the presence of long-range memory. For certain collections, a power-law decay can also be observed. These long-range autocorrelations persist for several hundred hours. A similar power-law decay in ACF was observed in a prior study³² for the most liquid collections on the Solana blockchain.

B. Detrended correlations

Given that the properties of the time series discussed in section II A were identified as heavy-tailed with a long memory, the detrended cross-correlation coefficient $\rho(q, s)$ ⁷⁰ was em-

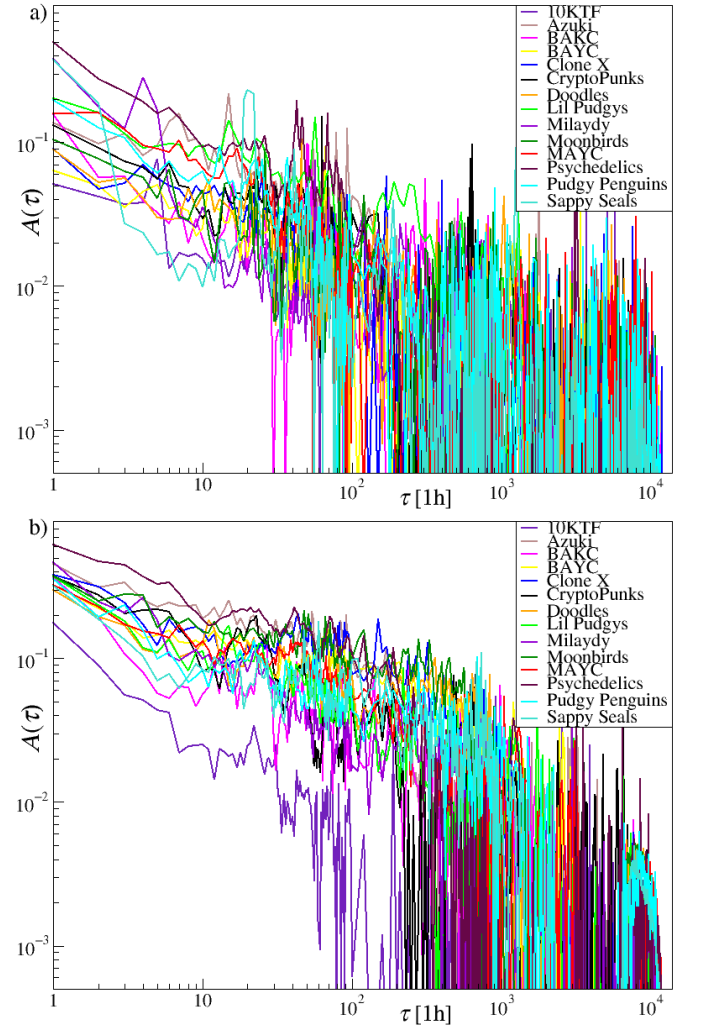


FIG. 4. Autocorrelation functions of $c_{\Delta t=1h}$ (a) and $N_{\Delta t=1h}$ (b) for all the collections.

ployed alongside the standard Pearson coefficient to compute correlations among the characteristics of the considered collections. The method used to derive $\rho(q, s)$ is the multifractal version of detrended fluctuation analysis (MFDFA)^{71,72}, which was designed to identify long-range power-law auto- and cross-correlations that give rise to trends across various time scales. Consequently, in contrast to the conventional trend-elimination techniques, MFDFA and the related measures such as the q -dependent detrended cross-correlation coefficient $\rho(q, s)$ are effective in managing nonstationarity⁷³. The coefficient $\rho(q, s)$ allows one for an examination of cross-correlation intensity across various time scales. The parameter q enables for the correlation analysis to focus on a specific range of fluctuation magnitudes.

The procedure for calculating the $\rho(q, s)$ coefficient consists of the following steps. Two time series $\{x(i)\}_{i=1, \dots, T}$ and $\{y(i)\}_{i=1, \dots, T}$ of length T are divided into M_s segments of length s starting from its opposite ends. Then the time series are integrated, and in each segment v , the polynomial trend is

removed:

$$X_v(s, i) = \sum_{j=1}^i x(vs + j) - P_{X,s,v}^{(m)}(i), \quad (2)$$

$$Y_v(s, i) = \sum_{j=1}^i y(vs + j) - P_{Y,s,v}^{(m)}(i), \quad (3)$$

where the polynomials $P^{(m)}$ of order m are utilized. Specifically, an order of $m = 2$ was chosen for its effectiveness with financial time series⁷⁴. Following this procedure, a total of $2M_s$ segments containing detrended signals are generated. Subsequently, the variance and covariance for each segment v are calculated as follows:

$$f_{ZZ}^2(s, v) = \frac{1}{s} \sum_{i=1}^s (Z_v(s, i))^2, \quad (4)$$

$$f_{XY}^2(s, v) = \frac{1}{s} \sum_{i=1}^s X_v(s, i) \times Y_v(s, i), \quad (5)$$

where Z means X or Y . These quantities are used to calculate a family of the fluctuation functions:

$$F_{ZZ}(q, s) = \frac{1}{2M_s} \sum_{v=0}^{2M_s-1} [f_{ZZ}^2(s, v)]^{q/2}, \quad (6)$$

$$F_{XY}(q, s) = \frac{1}{2M_s} \sum_{v=0}^{2M_s-1} \text{sign}[f_{XY}^2(s, v)] |f_{XY}^2(s, v)|^{q/2}, \quad (7)$$

where a sign function $\text{sign}[f_{XY}^2(s, v)]$ is maintained to ensure that outcomes remain consistent across various values of qs .

Finally, the formula for the q -dependent detrended correlation coefficient is presented as follows⁷⁰:

$$\rho^{XY}(q, s) = \frac{F_{XY}(q, s)}{\sqrt{F_{XX}(q, s)F_{YY}(q, s)}}. \quad (8)$$

For $q = 2$, the given definition can be interpreted as a detrended version of the Pearson cross-correlation coefficient C^{75} . In this context, the parameter q functions as a selective mechanism that either suppress ($q < 2$) or amplifies ($q > 2$) the fluctuation variance/covariance determined within the segments v in Eqs. (6) and (7). When $q < 2$, segments characterized by small fluctuations have a greater influence on $\rho_q(s)$, whereas, for $q > 2$, segments marked by large fluctuations have a heightened impact. Hence, utilizing this measure allows for the identification of the range of fluctuation sizes contributing to the noted correlations.

The methods presented above can also be used to investigate the presence of multifractality for a single time series. If the bivariate or univariate fluctuation functions can be approximated by a power-law relation

$$F(q, s) \sim s^{h(q)}, \quad (9)$$

where $h(q)$ represents a non-increasing function of q , known as the generalized Hurst exponent⁷⁶. This function indicates

that the analyzed time series exhibits a fractal structure. When $h(q)$ remains constant, the structure is identified as monofractal, with $h(q) = H$ being the Hurst exponent - a metric for time series persistence. If $h(q)$ is not constant, the structure is recognized as multifractal. The source of multifractality in the time series is the occurrence of non-linear correlations⁷⁷⁻⁸⁰, which are related to the existence of long memory manifested by power-law decay of the autocorrelation function. As observed in Fig. 4, such a power-law decay of the autocorrelation function occurs in the case of the considered collection time series. The multifractality of the financial time series is also a stylized fact^{73,81}. In our previous work³², the sign of multifractality of the NFT collections from the Solana blockchain time series characteristics was observed for some cases, especially for large fluctuations.

This study investigates the fractal characteristics of capitalization increments $c_{\Delta t=1h}$ and number of transactions $N_{\Delta t=1h}$ for the most liquid collection during the examined period - Mutant Ape Yacht Club. Fig. 5 presents $F(q, s)$ for both $c_{\Delta t}$ (top) and $N_{\Delta t}$ (bottom) time series in double-logarithmic scale with $-4 \leq q \leq 4$ and $10 \leq s \leq 1,200$. As can be seen in both cases, there is at least a decade-long scaling range long enough to determine the slope of $F(q = 2, s)$ (green line in Fig. 5) and, thus, to obtain the Hurst exponent $H \equiv h(q = 2)$ according to Eq. (9). The values indicate that both the analyzed time series are persistent with $H = 0.62 \pm 0.02$ for $c_{\Delta t}$ and $H = 0.65 \pm 0.02$ for $N_{\Delta t}$. These findings are in agreement with the results from our previous study based on NFT collections on the Solana blockchain³². However, when examining $h(q)$ across a range of $q \in [-4, 4]$, a sufficient scaling region is identifiable solely for the number of transactions (as it is highlighted by red dashed lines in the bottom panel of Fig. 5). For the capitalization increments, the scaling region is noticeable only for negative qs , and it does not extend beyond $q > 2$. Having calculated $h(q)$, it is straightforward to derive the singularity spectra $f(\alpha)$ in accordance to the following formulas:

$$\alpha = h(q) + q \frac{dh(q)}{dq}, \quad f(\alpha) = q(\alpha - h(q)) + 1. \quad (10)$$

The multifractal spectrum for the number of transactions $N_{\Delta t}$ is depicted in the inset of Fig. 5. Notably, the spectrum exhibits only the left branch indicating that the multifractal structure is evident only for medium and large fluctuations. For both $c_{\Delta t}$ and $N_{\Delta t}$, the negative qs that are associated with smaller fluctuations exhibit a monofractal regime indicated by the absence of a right arm in $f(\alpha)$. This left-side asymmetry in the singularity spectrum is commonly observed in financial time series where smaller fluctuations tend to represent noise, while the medium and large ones contain genuine information^{56,73,82-86}.

C. Correlation matrix

In order to study correlations between the time series representing $I = 90$ collections: the logarithmic increments of total collection capitalization $c_{\Delta t}$ and the number of transactions $N_{\Delta t}$, the correlation matrices \mathbf{C} and $\mathbf{C}^p(q, s)$ based on

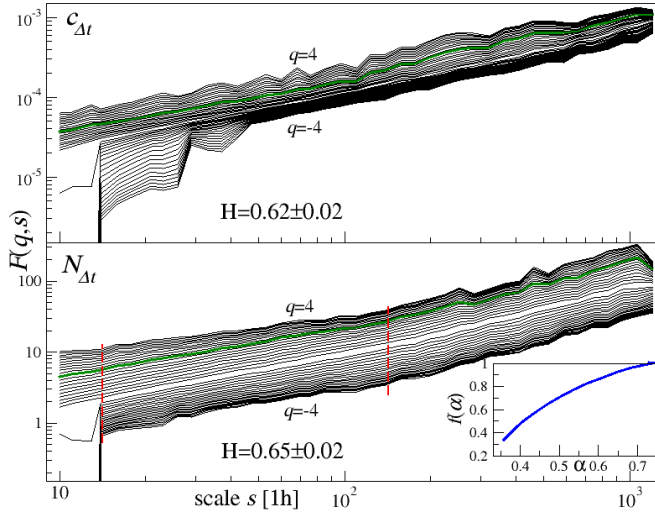


FIG. 5. Fluctuation functions $F(q, s)$ with $q \in [-4, 4]$ calculated for the number of transactions $N_{\Delta t} = 1h$ and logarithmic increments of the total collection capitalization $c_{\Delta t} = 1h$ for Mutant Ape Yacht Club collection. In main panels, thick green lines represent $F(q = 2, s)$, which are utilized in computation of the Hurst exponent H . Vertical red dashed lines point out to a scale range where the family of $F(q, s)$ exhibit power-law dependence for different values of q , from which the singularity spectrum $f(\alpha)$ can be calculated (insets).

the Pearson correlation coefficient⁸⁷ P_{ij} and the q -dependent detrended correlation coefficient⁷⁰ $\rho_{ij}(q, s)$ were created, respectively. After diagonalization of \mathbf{C} and \mathbf{C}^p :

$$\mathbf{C}\mathbf{v}_i = \lambda_i \mathbf{v}_i, \quad (11)$$

$$\mathbf{C}^p(q, s)\mathbf{v}_i^p(q, s) = \lambda_i^p(q, s)\mathbf{v}_i^p(q, s), \quad (12)$$

its eigenvalues λ_i , λ_i^p and eigenvectors $\mathbf{v}_i = \{v_{ij}\}$, $\mathbf{v}_i^p = \{v_{ij}^p\}$ are derived for $i, j = 1, \dots, I$. The resulting empirical eigenvalue distribution can be compared with the Marchenko-Pastur distribution linked to the Wishart ensemble⁸⁸ of random matrices \mathbf{W} . This ensemble exemplifies the inherent characteristics of uncorrelated independent and identically distributed (i.i.d.) random variables following a Gaussian distribution, $N(0, \sigma)$ ⁸⁹. The probability density function that describes the eigenvalue distribution of \mathbf{W} is given by⁹⁰

$$\phi_W(\lambda) = \frac{1}{I} \sum_{i=1}^N \delta(\lambda - \lambda_k) = \frac{Q}{2\pi\sigma_W^2} \frac{\sqrt{(\lambda_+ - \lambda)(\lambda - \lambda_-)}}{\lambda}, \quad (13)$$

$$\lambda_{\pm} = \sigma_W^2 \left(1 + 1/Q \pm 2\sqrt{\frac{1}{Q}}\right)$$

where $\lambda \in [\lambda_-, \lambda_+]$ and $Q = T/I$. Here, T and I denote the number of time series and their length, respectively. This relationship is strictly valid in the limit $T, K \rightarrow \infty$. However, contrasting an empirical eigenvalue distribution with the Marchenko-Pastur distribution helps in identifying the presence of any correlated patterns within the data.

III. CORRELATIONS BETWEEN COLLECTION CHARACTERISTICS

A. Eigenvalues and off-diagonal elements distributions

Properties of the correlation matrices derived from the time series of total collection capitalization increments $c_{\Delta t}$ and the number of transactions $N_{\Delta t}$ were analyzed and compared with theoretical predictions from the random matrix theory⁸⁸. The empirical eigenvalue distributions were compared with the Marchenko-Pastur distribution corresponding to the Wishart random matrix ensemble^{89,90} that represents the universal properties of uncorrelated i.i.d. random variables with a Gaussian distribution $N(0, 1)$. Moreover, the study included an examination of how the off-diagonal elements in the correlation matrices relate to a Gaussian distribution, enhancing the scope of the analysis.

In the Pearson-coefficient approach (upper panels of Fig. 6(a)), the number of eigenvalues exceeds the bounds of the Marchenko-Pastur (M-P) region, which contains the bulk of eigenvalues corresponding to random fluctuations. This fact points out to the presence of statistically significant correlations among the analyzed time series. Particularly noteworthy is the largest eigenvalue λ_1 , which stands well outside this region. This is a common phenomenon in the financial markets, where a typical eigenvalue spectrum of the Pearson-coefficient based correlation matrices consists of a large λ_1 , separated from the remaining ones by a considerable gap, that represents a collective market factor representing all the assets evolving in concert^{91,92}.

Mature financial markets are also characterized by the existence of a few other elevated non-random eigenvalues that correspond to market sectors (e.g., industries in the case of stock markets or geographical regions in the case of currencies)^{92,93}. Regarding both $c_{\Delta t}$ and $N_{\Delta t}$, it is observed that the eigenvalues λ_2 through λ_4 deviate from the M-P universal prediction, which is particularly noteworthy for λ_2 in the case of $N_{\Delta t}$. This suggests that the time series of the number of transactions are more closely correlated within groups than those for the capitalization increments. The significance of λ_2 becomes even more evident once the variance contribution associated with λ_1 has been filtered out by using a standard procedure^{91,94} (see top panels of Fig. 6(a)).

The market factor becomes weaker, although still significant, if the matrices $\mathbf{C}^p(q, s)$ are considered (middle panels of Fig 6(a) for $q = 1$ and bottom panels for $q = 4$). In this case, one could also observe an effect of the correlations increasing with time scale s , which is typical for the financial markets⁹⁵. The probability distribution function of the off-diagonal elements of the correlation matrices \mathbf{C} and $\mathbf{C}^p(q, s)$ offers complementary information to the eigenvalue distribution. Deviations from a Gaussian distribution in this case are visible in all the cases in Fig 6(b). The fattest tails are observed for $q = 4$ (large fluctuations) for $N_{\Delta t}$ - see bottom left panel of Fig 6(b), where the extreme elements $C_{ij}^p(q, s)$ exceed 0.9 even on the shortest time scale $s = 7$ days. These large correlations can be traced back to a number of transactions surge across various less-traded collections on the same day Jan, 6

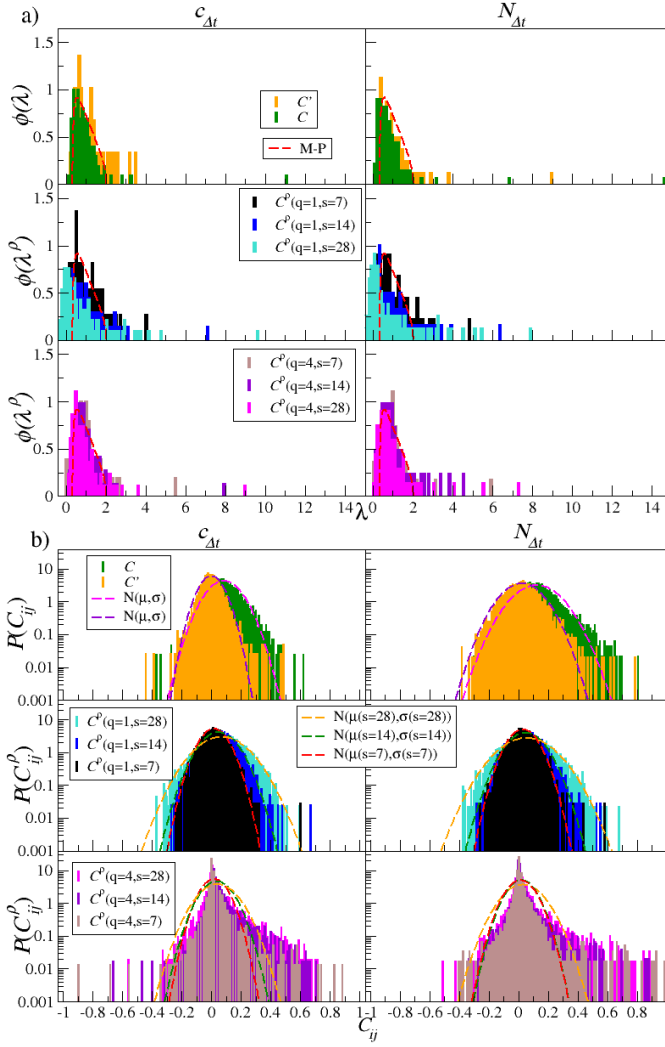


FIG. 6. (a) Eigenvalue distributions of the correlation matrices C (top) and $C^p(q, s)$ (middle for $q = 1$ and bottom for $q = 4$) created from the total collection capitalization increments $c_{\Delta t}$ (left) and the number of transactions $N_{\Delta t}$ (right) for $\Delta t = 1h$. The theoretical Marchenko–Pastur distribution $\phi_W(\lambda)$ is marked by dashed red lines. (b) Probability density functions of the off-diagonal elements of the same correlation matrices and data as in (a). Dashed lines show a fitted normal distribution to each empirical distribution (histograms).

2023 (inset of Fig. 1(b)). Their origin will be explained in the following section.

B. Eigenvector components

By examining the expansion coefficients v_{ij} of the eigenvectors \mathbf{v}_i associated with the eigenvalues λ_i that stand out significantly from the M-P region, it is possible to estimate their contributions by using either the Pearson or the detrended correlation coefficients derived from the time series of total collection capitalization increments $c_{\Delta t}$ and the number of transactions $N_{\Delta t}$ for λ_1 and λ_2 . In the case of $c_{\Delta t}$ and the Pearson correlation coefficient (top panel of Fig. 7), the collec-

tive character of \mathbf{v}_1 is distorted by the existence of the significant expansion coefficients v_{1j} with an opposite sign associated to: Lil Pudgys and Sappy Seals ($v_{1j} \approx -0.05$). On the other hand, the highest contribution to \mathbf{v}_1 comes from 3Landers, Karafuru and Alien Frens ($v_{1j} \in [0.18, 0.22]$). On the one hand, for $q = 1$ that corresponds to fluctuations of all magnitudes (Fig. 7, middle panel), the negative coefficients correspond to CyberKongz1, Metroverse and Killer GF collections, while for $q = 4$ that amplifies large fluctuations (Fig. 7, bottom panel), the negative expansion coefficients correspond to Acrocalypse and CyberKongz1 collections. On the other hand, the greatest contribution to $\mathbf{v}_1^p(q, s)$ is made by the expansion coefficients associated with Cool Cats, Goblintown, Alien Frens, and CrypToadz collections ($v_{1j}^p \in [0.18, 0.2]$) for $q = 1$ and with Chain Runners, Robotos, Galaxy Eggs, Alien Frens and Cool Cats collections ($v_{1j}^p \in [0.25, 0.31]$) for $q = 4$. It is worth noting that the largest v_{1j}^p are smaller for $q = 1$ than for $q = 4$ and for C .

A general conclusion that can be derived from the eigenvectors \mathbf{v}_1 and \mathbf{v}_1^p is that the most substantial contributions to the market factor do not originate from the most liquid and highly capitalized collections, such as Mutant Ape Yacht Club, Bored Ape Yacht Club, or CryptoPunks, but from less liquid collections with lower capitalization. This phenomenon can be attributed to the generally weak average correlation and, thus, to relatively minor significance of the market factor, as evidenced by the low values of the largest eigenvalue λ_1 and λ_1^p in relation to other financial markets⁹², including the cryptocurrency market⁹⁶. In fact, the source of the significant matrix elements was singular, exceptionally large synchronous events that occurred among less-liquid collections, like the activity rush on January 6, 2023.

In order to identify collections that contribute substantially to the eigenvector \mathbf{v}_2 , it is recommended to remove that part of the signal variance that corresponds to the largest eigenvalue λ_1 . It can be done by using a regression-based method^{91,92}:

$$c_{\Delta t}^{(i)}(k) = a^{(i)} + b^{(i)} Z_1(k) + \varepsilon^{(i)}(k),$$

$$Z_1(k) = \sum_{m=1}^I v_{1m} c_{\Delta t}^{(m)}(k), \quad (14)$$

where $Z_1(k)$ is the contribution to total variance associated with λ_1 ($k = 1, \dots, T$), and diagonalizing the filtered matrix C' constructed from the residual time series $\varepsilon^{(i)}(k)$ ($i = 1, \dots, I$). The corresponding eigenvalue-eigenvector pairs for such a filtered matrix have an index decreased by unity $\lambda_i \rightarrow \lambda'_{i-1}$, but for the sake of simplicity, we shall leave the index unchanged: $\lambda'_2, \mathbf{v}'_2$. Fig. 8 shows the expansion coefficients v_{2j} for the original matrix C without applying Eqs. (14) (top), for the filtered matrix C' (middle), and for the detrended correlation matrix $C^p(q, s)$ for $q = 4$ and $s = 14$ after filtering analogous to Eqs. (14) (bottom).

The first conclusion that can be drawn from the coefficients v_{2j} is that Pudgy Penguins and the collection originated from it - Lil Pudgys, that were created by the same producer - TheIglooCompany, show strong correlations in terms of $c_{\Delta t}$. The same applies to ape-themed collections (Bored Ape Yacht

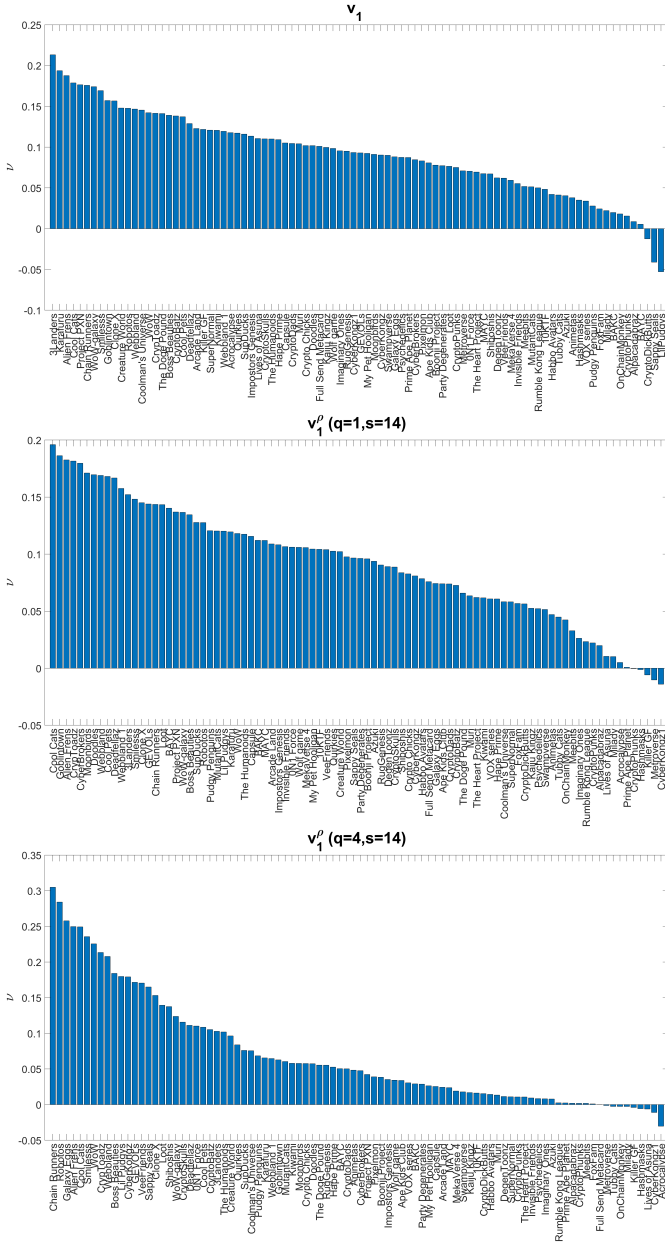


FIG. 7. Expansion coefficients of the eigenvector \mathbf{v}_1 associated with largest eigenvalue λ_1 of the Pearson correlation matrix \mathbf{C} (top) and of the eigenvectors $\mathbf{v}_1^p (q=1, s=14)$ and $\mathbf{v}_1^p (q=4, s=14)$ associated with largest eigenvalue $\lambda_1^p (q=1, s=14)$ (middle) and $\lambda_1^p (q=4, s=14)$ (bottom), respectively. All correlation matrices were calculated based on the total capitalization increment time series $c_{\Delta t}$.

Club, Bored Ape Kennel Club, and Mutant Ape Yacht Club) released by Yuga Labs. The related expansion coefficients are among the largest ones ($v_{2j} \in [0.2, 0.4]$), together with Sappy Seals (top panel of Fig. 8). The close relations among collections released by TheIglooCompany become even more pronounced after removing the contribution of λ_1 (middle panel of Fig. 8), where their expansion coefficients $v_{2j}^p \approx 0.38$ are much larger than for the other collections. The largest opposite-sign contribution to \mathbf{v}_2 , which indicates a different

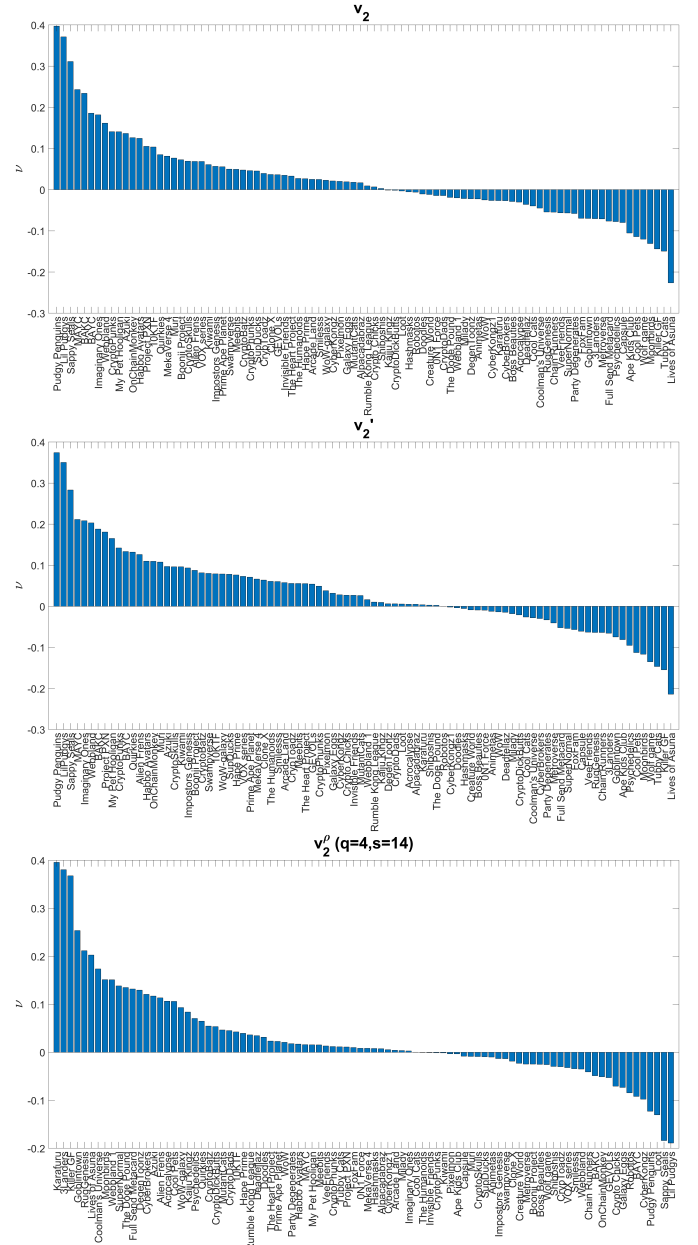


FIG. 8. Expansion coefficients of the eigenvector \mathbf{v}_2 associated with the 2nd largest eigenvalue λ_2 of the Pearson correlation matrix \mathbf{C} (top), the eigenvector \mathbf{v}_2' associated with the largest eigenvalue λ_2' of the filtered correlation matrix \mathbf{C}' (middle), and the eigenvector \mathbf{v}_2^p associated with the largest eigenvalue λ_2^p of the detrended correlation matrix $\mathbf{C}^p (q=4, s=14)$ (bottom). All correlation matrices were calculated based on the total capitalization increment time series $c_{\Delta t}$.

behavior, is observed for Lives of Asuna collection (middle panel of Fig. 8). Other relations between collections can be inferred from $\mathbf{v}_2^p (q=4, s=14)$ (bottom panel of Fig. 8) for $q=4$, which amplifies large fluctuation contribution to the cross-correlations. In this case, v_{2j}^p corresponding to Kara-furu, 3Landers, and Killer GF collections that fall in the range $v_{2j}^p \in [0.38, 0.4]$ and v_{2j}^p corresponding to Goblintown that is

equal to $v_{2j}^p \approx 0.25$ show significantly different values than the average $|v_{2j}^p| < 0.2$ observed for the other collections. These less-liquid collections experienced a significant drop in capitalization on January 6, 2023, which was also accompanied by an increased number of transactions (inset in Fig 1(b)). The strongest opposite-sign contributions to \mathbf{v}_2^p are made by Lil Pudgys and Sappy Seals ($v_{2j}^p \in [-0.15, -0.2]$).

For the number of transactions time series $N_{\Delta t}$ the results for the expansion coefficients (not shown) differ in that here, for \mathbf{C} their largest values correspond to the most liquid collections: Mutant Ape Yacht Club, Pudgy Penguins, Bored Ape Yacht Club, Moonbirds, Clone X, Azuki, ON1 Force, and Milady Maker ($v_{2j} \in [0.15, 0.25]$). This is confirmed by the large expansion coefficients of the eigenvector \mathbf{v}_2' calculated for the filtered matrix \mathbf{C}' , which - despite a slightly different order - form a similar liquid-collection cluster. The largest opposite-sign coefficients $v_{2j} \in [-0.15, -0.2]$ are associated with the least liquid collections: CryptoBatz, Webbland, Coolman's Universe, Smilesss, Project PXN, and 3Landers, while the largest opposite-sign coefficients $v_{2j}' \in [-0.16, -0.22]$ are associated with 3Landers, Alien Frens, Project PXN, Coolman's Universe, Killer GF, CryptoBatz, and Smilesss. In contrast, the expansion coefficients for $\mathbf{C}^p(q=4, s=14)$ are dominated by less-liquid collections: Alien Frens, Killer GF, 3Landers, and Coolman's Universe ($v_{2j}^p \in [0.2, 0.31]$), which experienced significant increase in the number of transactions on January 6, 2023. The largest opposite-sign contributions to \mathbf{v}_2^p correspond to the following collections: CyberKongz, Hashmasks, and Mutant Ape Yacht Club ($v_{2j}^p \in [-0.3, -0.2]$).

C. Minimal spanning trees (MST)

A correlation matrix can be used to form a weighted network where nodes represent collections and edges represent correlations⁵⁰. However, if the number of nodes is significant, such complete networks are difficult to comprehend when plotted and, for the sake of graphical clarity, another useful network representation is recommended, which is minimal spanning tree (MST). It is a subnetwork consisting of I nodes and $I - 1$ edges and its key property is that it minimizes the sum of edge weights. In order to create MST, the correlation matrices \mathbf{C} and $\mathbf{C}^p(q, s)$ must be transformed into distance matrices \mathbf{D} and $\mathbf{D}^p(q, s)$, respectively, where the entries, calculated according to the following formula:

$$d_{ij} = \sqrt{2(1 - P_{ij})}, \quad d_{ij}^p(q, s) = \sqrt{2(1 - \rho_{ij}(q, s))}, \quad (15)$$

are metric distances. The edges minimizing their weight sum are then selected according to Kruskal's or Prim's algorithm^{97,98}. From the present work's perspective the structure of an MST can offer a useful insight into the cross-correlation patterns within a market. For instance, a centralized market would be characterized by a star-shaped tree, whereas a market with idiosyncratic dynamics of assets would be characterized by a decentralized structure with extended branches and no significant hub.

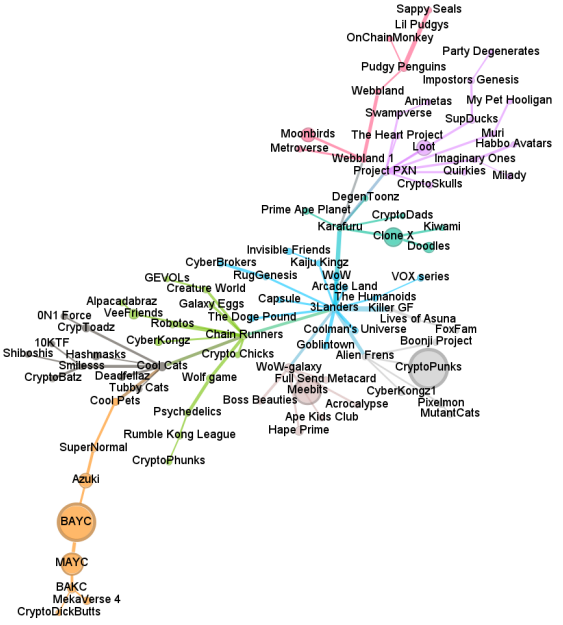


FIG. 9. MST based on the Pearson correlation matrix \mathbf{C} for the capitalization increments $c_{\Delta t}$ of different collections. Symbols representing nodes have their size reflecting the collection capitalization on the last day of the period of interest, while node colors denote the communities identified by means of the Louvain method⁹⁹. Edge thickness shows correlation strength.

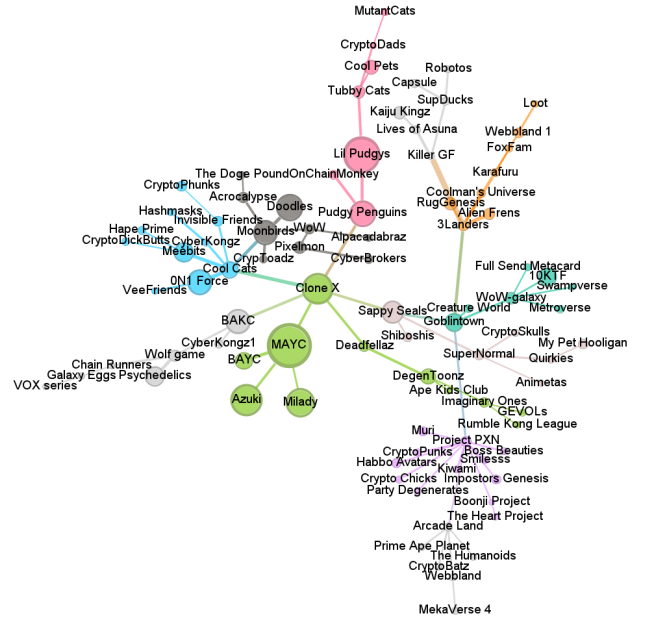


FIG. 10. Similar MST as in Fig. 9 but for the number of transactions time series $N_{\Delta t}$ and node size represents the total number of transactions in the considered period.

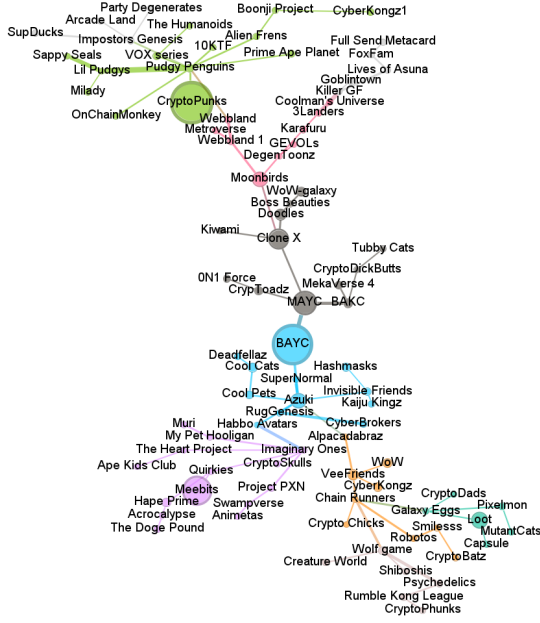


FIG. 11. MST for the same $c_{\Delta t}$ dataset as in Fig. 9 but for the filtered correlation matrix C' for the original time series.

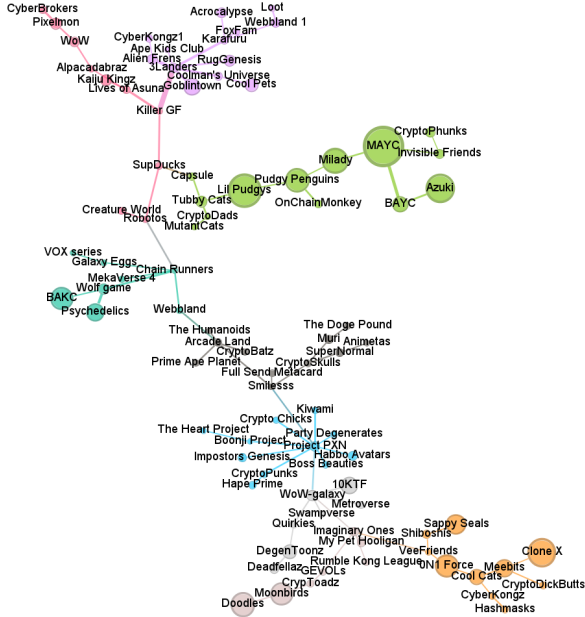


FIG. 12. MST for the same $N_{\Delta t}$ dataset as in Fig. 10 but for the filtered correlation matrix C' for the original time series.

The MST presented in Fig. 9 was constructed from the correlation matrix C based on the Pearson coefficients between the time series of the collection capitalization increments $c_{\Delta t}$. The MST is characterized by a rather distributed structure with no dominant hub. This remains in agreement with the observation coming out of Fig. 7 that the market factor rep-

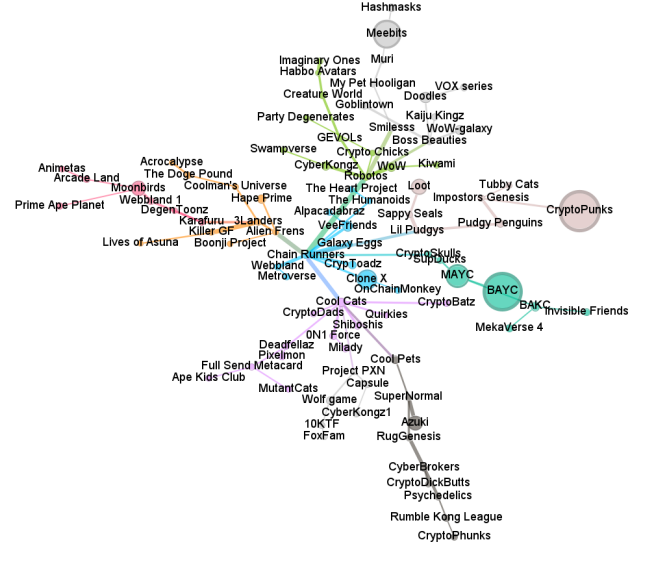


FIG. 13. MST based on the q -dependent detrended correlation matrix $C^p(q, s)$ for $q = 4$ and $s = 14$ for the capitalization increments $c_{\Delta t}$.

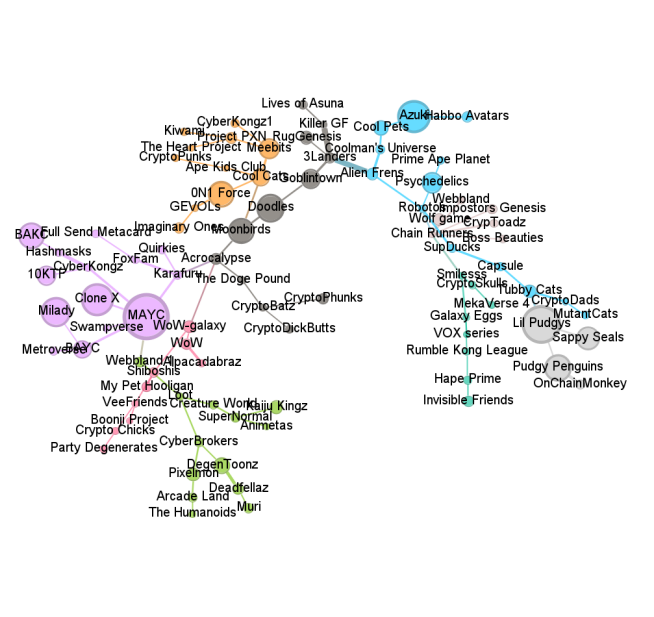


FIG. 14. MST based on the q -dependent detrended correlation matrix $C^p(q, s)$ for $q = 4$ and $s = 14$ for the number of transactions $N_{\Delta t}$.

resented by \mathbf{v}_1 does not comprise all the collections with the same strength. The strongest local center is the node corresponding to 3Landers with a degree of $\delta = 14$, which is also the central node for a community of 15 collections. Among other minor centers one can point out to Project PXN, Karafuru, Chain Runners, and Cool Cats. This is remarkably dif-

ferent than in the case of other financial markets like the stock market, Forex, or cryptocurrency market where the structure is predominantly centralized with a well-distinguished hub^{41,56,96}. Such a structure is not restricted to capitalization data, but also occurs in the case of the number of transactions $N_{\Delta t}$ – see Fig. 10. Here the most connected node, which is Project PXN, has degree of $\delta = 12$ and there exist a few other small centers like 3Landers, Cool Cats and Clone X.

It is interesting to look at the MST structure after removing the variance component corresponding to λ_1 . For both $c_{\Delta t}$ (Fig. 11) and $N_{\Delta t}$ (Fig. 12), MST remains decentralized as one might expect from the structure of the corresponding eigenvector \mathbf{v}_2 in Fig. 8. The most connected nodes are Pudgy Penguins for $c_{\Delta t}$ and Project PXN for $N_{\Delta t}$, both with $\delta = 10$. The secondary cluster centers are Azuki for $c_{\Delta t}$ and 3Landers for $N_{\Delta t}$, both with $\delta = 7$.

The $c_{\Delta t}$ -based MST created from $\mathbf{C}^p(q, s)$ for $q = 4$ and $s = 14$ focuses on the correlation structure among large capitalization increments. Consistently with the fat-tailed distribution of the matrix elements depicted in Fig. 6(b), where there are few large elements and many small ones, the MST reveals a distributed structure with a few small clusters centered at Chain Runners ($\delta = 11$), Robotos ($\delta = 9$) and Cool Cats ($\delta = 7$) – see Fig. 13. An evident property of the MSTs for $c_{\Delta t}$ is that the nodes corresponding to the collections with the largest capitalization (large circles), with the exception of the Ape collections, do not cluster together. Especially the collection with the largest capitalization – CryptoPunks – is peripheral in all the cases. This effect can be viewed as a contrasting one in respect to the other financial markets, where the largest stocks, currencies, and cryptocurrencies were identified as central nodes^{41,56,92,96}. For $N_{\Delta t}$, the corresponding MST is even more dispersed with the most connected nodes being Chain Runners ($\delta = 7$) and Mutant Ape Yacht Club ($\delta = 6$) – see Fig. 14. The cluster centered around the latter contains the collections with the largest number of transactions.

The decentralized structure of the MSTs presented in Figs. 9-14 can also be inferred from the node degree cumulative distributions shown in Fig. 15 where no node stands out as an outlier. In the case of the MSTs based on \mathbf{C} (top panels), even a trace of a power-law dependence can be seen (straight lines in the double logarithmic scale plots). Such distributions of δ define the scale-free networks¹⁰⁰ and were also reported for foreign currency exchange rates⁵⁴ and cryptocurrencies^{41,55}. No similar result can be seen for $\mathbf{C}^p(q, s)$ for $q = 1$ (middle panels) and $q = 4$ (bottom panels).

IV. SUMMARY

Despite its young age and unique trading dynamics, the NFT market exhibits many similarities with the cryptocurrency market and the traditional financial markets like the stock market and Forex. Among such similarities one can point out to long range memory and fat tailed probability distribution functions of some observables (e.g., absolute values of logarithms of the capitalization increments and the num-

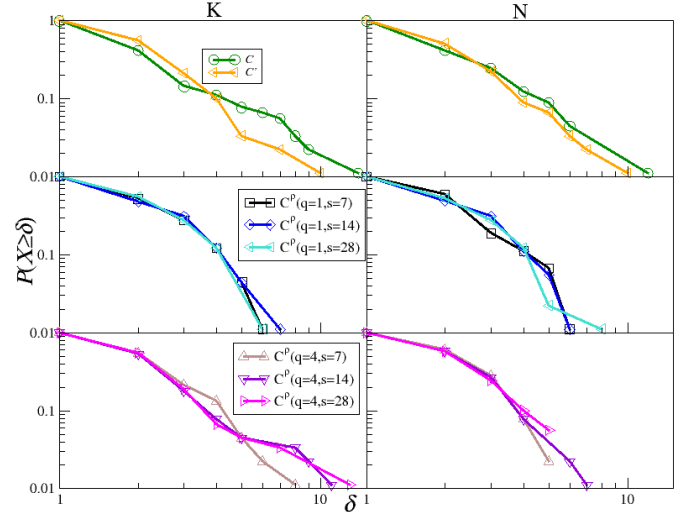


FIG. 15. Cumulative distribution function $P(X \geq \delta)$ of the node degrees δ of MSTs created from the collection capitalization increments $c_{\Delta t}$ (left) and the number of transactions $N_{\Delta t}$ (right). The correlation matrices based on the Pearson coefficients \mathbf{C} (top) and the q -dependent detrended correlation coefficients $\mathbf{C}^p(q, s)$ for $q = 1$ (middle) and $q = 4$ (bottom) were used.

ber of transactions in time unit). However, there are differences as well. The collection cross-correlations tend to be lower than their counterparts in the other markets, which manifests itself in the magnitude of the largest eigenvalue λ_1 of the corresponding correlation matrices (both those based on the Pearson correlations and the q -dependent detrended ones), yet they markedly deviate from random ones. Another difference is the fact that only a fraction of the total number of the collections contribute to a market factor, while the remaining ones show more independent behavior and can be grouped in clusters. Moreover, there is a significant negative contribution of some collections to the overall dynamics, which is quantified in the negative vector expansion coefficients in the eigenvector related to λ_1 . Such anti-correlation was not so frequently observed in the case of cryptocurrencies, for example. Another interesting atypical property of the NFT market is strong cross-correlations between large fluctuations of the studied observables among less liquid collections, especially in the case of the number of transactions in time unit.

An additional insight into the cross-correlation structure of the NFT market has been given by a network approach that utilized minimal spanning trees. They reveal a largely decentralized structure of the respective MSTs that lack a dominant node, which remains in a striking contrast with the cryptocurrency market not to mention the traditional markets. Despite the fact that there exist large discrepancies in capitalization of the collections and the number of transactions, the price evolution of the largest, most frequently traded collections do not necessarily impact the respective characteristics of the less priced collections. This is yet another disparity between the NFT collections and the other financial assets, where the highly capitalized assets dominate the evolution of a market and tend to be coupled to each other.

These differences go far beyond a lesser maturity and the associated lower liquidity of the NFT assets and they could stem from the unique trading mechanisms that are distinct from those in the other markets. For example, there is no order book here and, what is even more important, token non-fungibility makes performing simple arbitrage impossible. Consequently, the information transmission mechanism is slower both within the same collection and between different collections. All these factors lead to the observed weaker cross-correlations among the tokens than in the case of cryptocurrencies and traditional financial assets.

ACKNOWLEDGMENTS

This research was funded in whole or in part by National Science Centre, Poland 2023/07/X/ST6/01569.

DATA AVAILABILITY STATEMENT

The data is freely available from CryptoSlam!⁵⁹ portal.

V. APPENDIXES

¹S. Nakamoto, "Bitcoin: A peer-to-peer electronic cash system," , 1–9 (2009).

²F. A. Sunny, P. Hajek, M. Munk, M. Z. Abedin, M. S. Satu, M. I. A. Efat, and M. J. Islam, "A systematic review of blockchain applications," *IEEE Access* **10**, 59155–59177 (2022).

³ETH, <https://ethereum.org/whitepaper>.

⁴ERC-20 protocol, <https://eips.ethereum.org/EIPS/eip-20>.

⁵M. Rosenfeld, "Overview of colored coins," (2012).

⁶quantmNFT, "quantmNFT," <https://nftnow.com/art/quantum-the-first-piece-of-nft-art-ever-created>.

⁷C. Bellón and I. Figuerola-Ferretti, "Bubbles in ethereum," *Finance Research Letters* **46**, 102387 (2022).

⁸X.-J. Jiang and X. F. Liu, "Cryptokitties transaction network analysis: The rise and fall of the first blockchain game mania," *Frontiers in Physics* **9** (2021).

⁹ERC-721 protocol, <https://eips.ethereum.org/EIPS/eip-721>.

¹⁰Y. Maouchi, L. Charfeddine, and G. El Montasser, "Understanding digital bubbles amidst the COVID-19 pandemic: Evidence from DeFi and NFTs," *Finance Research Letters* **47**, 102584 (2022).

¹¹TVL, <https://coinmarketcap.com/chain-ranking/>.

¹²S. W. Mingjun Guo and Y. Wei, "Bubbles in NFT markets: correlated with cryptocurrencies or sentiment indexes?" *Applied Economics Letters* **0**, 1–7 (2023).

¹³Christies Press Center, <https://www.christies.com/about-us/press-archive/details?PressReleaseID=9970>.

¹⁴F. Horky, L. Dubbick, F. Rhein, and J. Fidrmuc, "Don't miss out on NFTs?! A sentiment-based analysis of the early NFT market," *International Review of Economics & Finance* **88**, 799–814 (2023).

¹⁵H. M. Kim and S. Chakraborty, "Exploring the diffusion of digital fashion and influencers' social roles in the Metaverse: an analysis of Twitter hashtag networks," *Internet Research* **34**, 107–128 (2024).

¹⁶NFTceleb, <https://www.techopedia.com/celebrity-nfts-10-famous-personalities-who-launched-their-own-digital-tokens>.

¹⁷TrumpNFT, <https://www.businessinsider.com/trump-major-announcement-digital-trading-card-nfts-2022-12>.

¹⁸NFTbubble, <https://www.forbes.com/sites/digital-assets/2023/11/10/nfts-are-retaining-value-researchers-say>.

¹⁹NFTcrash, <https://supra.com/academy/nft-market-crash/>.

²⁰coinmarketcap, <https://coinmarketcap.com/nft/>.

²¹P. Bose, D. Das, F. Gritti, N. Ruaro, C. Kruegel, and G. Vigna, "Exploiting unfair advantages: Investigating opportunistic trading in the NFT market," (2023).

²²I. Sifat, S. A. Tariq, and D. van Donselaar, "Suspicious trading in non-fungible tokens (NFTs)," *Information & Management* **61**, 103898 (2024).

²³V. von Wachter, J. R. Jensen, F. Regner, and O. Ross, "NFT Wash Trading: Quantifying suspicious behaviour in NFT markets," (2022), <http://arxiv.org/abs/2202.03866>.

²⁴P. Bose, D. Das, F. Gritti, N. Ruaro, C. Kruegel, and G. Vigna, "Exploiting unfair advantages: Investigating opportunistic trading in the NFT market," (2024), <https://arxiv.org/abs/2310.06844>.

²⁵BTCordinals, <https://docs.ordinals.com/>.

²⁶Blokchianshare, <https://www.coingecko.com/research/publications/market-share-nft-blockchains>.

²⁷NFTmarketplaces, <https://dappradar.com/rankings/nft/marketplaces>.

²⁸NFTcrit, <https://markets.businessinsider.com/news/currencies/ethereum-vitalik-buterin-crypto-bored-ape-yacht-club-nft-wealth-2022-3>.

²⁹O. Ali, M. Momin, A. Shrestha, R. Das, F. Alhajj, and Y. K. Dwivedi, "A review of the key challenges of non-fungible tokens," *Technological Forecasting and Social Change* **187**, 122248 (2023).

³⁰D. Chalmers, C. Fisch, R. Matthews, W. Quinn, and J. Recker, "Beyond the bubble: Will NFTs and digital proof of ownership empower creative industry entrepreneurs?" *Journal of Business Venturing Insights* **17**, e00309 (2022).

³¹C. Giannoni, F. Medda, and S. Bartolucci, "Blockchain technologies and art: Opportunities and open challenges," (2023), <https://ssrn.com/abstract=4439318>.

³²P. Szydło, M. Wątopek, J. Kwapien, and S. Drożdż, "Characteristics of price related fluctuations in non-fungible token (NFT) market," *Chaos* **34**, 013108 (2024).

³³N. James and M. Menzies, "Efficiency of communities and financial markets during the 2020 pandemic," *Chaos* **31**, 083116 (2021).

³⁴N. James, M. Menzies, and G. A. Gottwald, "On financial market correlation structures and diversification benefits across and within equity sectors," *Physica A* **604**, 127682 (2022).

³⁵S. Drożdż, A. Górski, and J. Kwapien, "World currency exchange rate cross-correlations," *The European Physical Journal B* **58**, 499–502 (2007).

³⁶R. Gębarowski, P. Oświęcimka, M. Wątopek, and S. Drożdż, "Detecting correlations and triangular arbitrage opportunities in the Forex by means of multifractal detrended cross-correlations analysis," *Nonlinear Dynamics* **98**, 2349–2364 (2019).

³⁷J. Miśkiewicz, "Network analysis of cross-correlations on Forex market during crises. globalisation on Forex market," *Entropy* **23** (2021).

³⁸D. Stosic, D. Stosic, T. B. Ludermit, and T. Stosic, "Collective behavior of cryptocurrency price changes," *Physica A* **507**, 499–509 (2018).

³⁹H. Chaudhari and M. Crane, "Cross-correlation dynamics and community structures of cryptocurrencies," *Journal of Computational Science* **44**, 101130 (2020).

⁴⁰S. Drożdż, L. Minati, P. Oświęcimka, M. Stanuszek, and M. Wątopek, "Competition of noise and collectivity in global cryptocurrency trading: Route to a self-contained market," *Chaos* **30**, 023122 (2020).

⁴¹M. Wątopek, S. Drożdż, J. Kwapien, L. Minati, P. Oświęcimka, and M. Stanuszek, "Multiscale characteristics of the emerging global cryptocurrency market," *Physics Reports* **901**, 1–82 (2021).

⁴²N. James and M. Menzies, "Collective correlations, dynamics, and behavioural inconsistencies of the cryptocurrency market over time," *Nonlinear Dynamics* **107**, 4001–4017 (2022).

⁴³A. P. N. Nguyen, T. T. Mai, M. Bezbradica, and M. Crane, "The cryptocurrency market in transition before and after COVID-19: An opportunity for investors?" *Entropy* **24** (2022).

⁴⁴J. Gavin and M. Crane, "Community detection in cryptocurrencies with potential applications to portfolio diversification," in *FinTech Research and Applications: Challenges and Opportunities* (World Scientific, 2023) pp. 177–202.

⁴⁵N. James and M. Menzies, "Collective dynamics, diversification and optimal portfolio construction for cryptocurrencies," *Entropy* **25** (2023).

TABLE I. NFT collections considered in this study. K - collection capitalization on the last day from the dataset, N_{tot} - total number of transactions, S - collection size measured by the number of circulated tokens, and $\%0_{\Delta t=1h}$ - the fraction of hours without transactions.

Name	$K[10^6\$]$	N_{tot}	S	$\%0_{\Delta t=1h}$	Name	$K[10^6\$]$	N_{tot}	S	$\%0_{\Delta t=1h}$
0N1 Force	51.3	28565	7766	54%	Invisible Friends	47.3	7432	4931	67%
10KTF	21.8	18901	25826	46%	Kaiju Kingz	35.1	10986	7289	55%
3Landers	29.4	7498	8650	69%	Karafuru	34.1	4801	5415	77%
Acrocalypse	9.4	8302	10010	74%	Killer GF	20.3	2944	6618	85%
Alien Frens	28.3	8778	9569	58%	Kiwami	18.8	3313	9392	84%
Alpacadabraz	17.0	2965	9287	87%	Lil Pudgys	10.5	44984	17853	28%
Animetas	16.1	1911	9672	91%	Lives of Asuna	18.6	5117	9771	80%
Ape Kids Club	19.8	1688	9466	92%	Loot	323.8	2553	6153	91%
Arcade Land	38.2	5040	8677	76%	Meebits	724.1	20741	13345	53%
Azuki	292.1	37565	9718	36%	MekaVerse 4	77.3	3151	8576	85%
Boonji Project	20.0	1588	11004	91%	Metroverse City Block	29.1	3969	8930	85%
Bored Ape Kennel Club (BAKC)	105.5	27892	7227	43%	Milady	31.1	33123	8466	41%
Bored Ape Yacht Club (BAYC)	1082.7	17383	9290	48%	Moonbirds	291.3	27797	8747	48%
Boss Beauties	21.3	3117	8858	83%	Muri	21.5	6188	9926	76%
Capsule	28.9	4899	9668	85%	Mutant Ape Yacht Club (MAYC)	559.5	55694	15809	18%
Chain Runners	28.3	2204	9915	91%	MutantCats	22.5	3340	9940	89%
Clone X	445.8	36962	12076	31%	My Pet Hooligan	20.3	6617	7779	68%
Cool Cats	106.8	16948	8840	54%	OnChainMonkey	25.6	5422	8244	75%
Cool Pets	75.2	13299	14377	78%	Party Degenerates	22.0	3035	9705	88%
Coolman's Universe	24.8	5269	9130	55%	Pixelmon	47.5	10499	9549	70%
Creature World	37.3	4298	9814	80%	Prime Ape Planet	45.7	3183	7598	86%
Crypto Chicks	14.6	2863	9944	78%	Project PXN	32.9	7878	9453	66%
CrypToadz	84.0	4107	6452	83%	Psychedelics Anonymous Genesis	25.5	20876	9474	47%
CryptoBatz by Ozzy Osbourne	28.2	3158	8734	86%	Pudgy Penguins	70.9	29869	8897	41%
CryptoDads	17.4	2168	9872	89%	Quirkies	16.9	4529	4735	79%
CryptoDickButts S3	14.6	4108	5140	81%	Robotos	19.1	2624	9885	87%
CryptoPhunks V2	27.4	7813	7450	73%	RugGenesis	19.6	10554	17200	67%
CryptoPunks	1147.4	2964	6960	83%	Rumble Kong League	34.1	2612	9897	87%
CryptoSkulls	24.4	3283	7680	81%	Sappy Seals	13.9	24449	9737	48%
CyberBrokers	53.4	4930	7744	79%	Shiboshis	26.1	5767	6882	73%
CyberKongz VX 1	51.2	4734	11952	82%	Smilesss	15.7	2565	7296	87%
CyberKongz	100.3	3101	3304	77%	SupDucks	27.4	4131	9950	79%
Deadfellaz	33.0	8139	9197	61%	SuperNormalbyZipcy	24.7	6057	7222	79%
DegenToonz	14.2	14989	8210	56%	Swampverse	11	2321	9523	91%
Doodles	174.0	30860	8690	45%	The Heart Project	15.1	2003	9651	83%
FoxFam	15.3	3189	9836	87%	The Humanoids	18.4	2406	9802	91%
Full Send Metacard	27.6	3452	9315	82%	The Doge Pound	39.6	3030	9919	87%
Galaxy Eggs	20.4	2547	9135	89%	Tubby Cats	22.7	10509	19468	70%
GEVOLs	14.5	2817	8478	85%	VeeFriends	149.8	2464	9106	85%
Goblintown	28.3	19183	8986	57%	VOX Series 1	53.3	2050	8702	87%
Habbo Avatars	12.3	6836	10610	67%	Webbland 1	39.2	6975	9058	85%
Hape Prime	100.2	4550	7068	77%	Webbland	34.9	3346	8498	79%
Hashmasks	84.5	3527	16336	84%	Wolf Game	55.7	9233	11518	70%
Imaginary Ones	21.0	6805	8456	71%	World of Women Galaxy (WoW-galaxy)	115.4	9542	14360	71%
Impostors Genesis	37.5	6222	9656	69%	World of Women (WoW)	102.2	7415	9397	58%

⁴⁶L. Laloux, P. Cizeau, J.-P. Bouchaud, and M. Potters, "Noise dressing of financial correlation matrices," *Physical Review Letters* **83**, 1467–1470 (1999).

⁴⁷V. Plerou, P. Gopikrishnan, B. Rosenow, L. A. Nunes Amaral, and H. E. Stanley, "Universal and nonuniversal properties of cross correlations in financial time series," *Physical Review Letters* **83**, 1471–1474 (1999).

⁴⁸S. Drożdż, J. Kwapień, F. Grümm, F. Ruf, and J. Speth, "Quantifying the dynamics of financial correlations," *Physica A* **299**, 144–153 (2001).

⁴⁹R. Mantegna, "Information and hierarchical structure in financial markets," *Computer Physics Communications* **121-122**, 153–156 (1999).

⁵⁰M. Tumminello, F. Lillo, and R. N. Mantegna, "Correlation, hierarchies, and networks in financial markets," *Journal of economic behavior & organization* **75**, 40–58 (2010).

⁵¹S. Miccichè, G. Bonanno, F. Lillo, and R. N. Mantegna, "Degree stability of a minimum spanning tree of price return and volatility," *Physica A* **324**, 66–73 (2003), proceedings of the International Econophysics Conference.

⁵²M. Wiliński, A. Sienkiewicz, T. Gubiec, R. Kutner, and Z. Struzik, "Structural and topological phase transitions on the German Stock Exchange," *Physica A* **392**, 5963–5973 (2013).

⁵³J. Miśkiewicz and D. Bonarska-Kujawa, "Evolving network analysis of S&P500 components: COVID-19 influence of cross-correlation network structure," *Entropy* **24** (2022), 10.3390/e24010021.

⁵⁴A. Z. Górski, S. Drożdż, and J. Kwapień, "Scale free effects in world currency exchange network," *The European Physical Journal B* **66**, 91–96

- (2008).
- ⁵⁵K. Polovnikov, V. Kazakov, and S. Syntulsky, “Core-periphery organization of the cryptocurrency market inferred by the modularity operator,” *Physica A* **540**, 123075 (2020).
 - ⁵⁶S. Drożdż, J. Kwapień, and M. Wątopek, “What is mature and what is still emerging in the cryptocurrency market?” *Entropy* **25** (2023).
 - ⁵⁷E. Brigatti, V. Rocha Grecco, A. Hernández, and M. Bertella, “Inferring interactions in multispecies communities: The cryptocurrency market case,” *Plos one* **18**, e0291130 (2023).
 - ⁵⁸A. P. N. Nguyen, T. T. Mai, M. Bezbradica, and M. Crane, “Volatility and returns connectedness in cryptocurrency markets: Insights from graph-based methods,” *Physica A* **632**, 129349 (2023).
 - ⁵⁹CryptoSlam, “Cryptoslam,” <https://www.cryptoslam.io>.
 - ⁶⁰miladyMusk, “miladymusk,” <https://cointelegraph.com/news/milady-nft-floor-price-surges-after-elon-musk-tweet>.
 - ⁶¹T. G. Andersen and T. Bollerslev, “Answering the skeptics: Yes, standard volatility models do provide accurate forecasts,” *International Economic Review* **39**, 885–905 (1998).
 - ⁶²G. Andersen, T. Bollerslev, and S. Lange, “Forecasting financial market volatility: Sample frequency vis-a-vis forecast horizon,” *Journal of Empirical Finance* **6**, 457–477 (1999).
 - ⁶³T. Bollerslev, J. Cai, and F. M. Song, “Intraday periodicity, long memory volatility, and macroeconomic announcement effects in the US Treasury bond market,” *Journal of Empirical Finance* **7**, 37–55 (2000).
 - ⁶⁴M. Wątopek, M. Skupień, J. Kwapień, and S. Drożdż, “Decomposing cryptocurrency high-frequency price dynamics into recurring and noisy components,” *Chaos* **33**, 083146 (2023).
 - ⁶⁵M. Ausloos, “Statistical physics in foreign exchange currency and stock markets,” *Physica A* **285**, 48–65 (2000).
 - ⁶⁶R. Cont, “Empirical properties of asset returns: stylized facts and statistical issues,” *Quantitative Finance* **1**, 223–236 (2001).
 - ⁶⁷V. Plerou, H. E. Stanley, X. Gabaix, and P. Gopikrishnan, “On the origin of power-law fluctuations in stock prices,” *Quantitative Finance* **4**, 11–15 (2004).
 - ⁶⁸M. Wątopek, J. Kwapień, and S. Drożdż, “Financial return distributions: Past, present, and COVID-19,” *Entropy* **23** (2021).
 - ⁶⁹P. Gopikrishnan, V. Plerou, L. A. Nunes Amaral, M. Meyer, and H. E. Stanley, “Scaling of the distribution of fluctuations of financial market indices,” *Physical Review E* **60**, 5305–5316 (1999).
 - ⁷⁰J. Kwapień, P. Oświęcimka, and S. Drożdż, “Detrended fluctuation analysis made flexible to detect range of cross-correlated fluctuations,” *Physical Review E* **92**, 052815 (2015).
 - ⁷¹C.-K. Peng, S. V. Buldyrev, S. Havlin, M. Simons, H. E. Stanley, and A. L. Goldberger, “Mosaic organization of dna nucleotides,” *Physical Review E* **49**, 1685–1689 (1994).
 - ⁷²J. W. Kantelhardt, S. A. Zschiegner, E. Koscielny-Bunde, S. Havlin, A. Bunde, and H. E. Stanley, “Multifractal detrended fluctuation analysis of nonstationary time series,” *Physica A* **316**, 87–114 (2002).
 - ⁷³Z. Q. Jiang, W. J. Xie, W. X. Zhou, and D. Sornette, “Multifractal analysis of financial markets: A review,” *Reports on Progress in Physics* **82**, 125901 (2019).
 - ⁷⁴P. Oświęcimka, S. Drożdż, J. Kwapień, and A. Z. Górski, “Effect of detrending on multifractal characteristics,” *Acta Physica Polonica A* **123**, 597–603 (2013).
 - ⁷⁵G. F. Zebende, “DCCA cross-correlation coefficient: Quantifying level of cross-correlation,” *Physica A* **390**, 614–618 (2011).
 - ⁷⁶A.-L. Barabasi and T. Vicsek, “Multifractality of self-affine fractals,” *Physical Review A* **44**, 2730–2733 (1991).
 - ⁷⁷S. Drożdż, J. Kwapień, P. Oświęcimka, and R. Rak, “Quantitative features of multifractal subtleties in time series,” *EPL* **88**, 60003 (2009).
 - ⁷⁸W.-X. Zhou, “The components of empirical multifractality in financial returns,” *Europhysics letters* **88**, 28004 (2009).
 - ⁷⁹R. Rak and D. Grech, “Quantitative approach to multifractality induced by correlations and broad distribution of data,” *Physica A* **508**, 48–66 (2018).
 - ⁸⁰J. Kwapień, P. Blasiak, S. Drożdż, and P. Oświęcimka, “Genuine multifractality in time series is due to temporal correlations,” *Physical Review E* **107**, 034139 (2023).
 - ⁸¹R. Kutner, M. Ausloos, D. Grech, T. Di Matteo, C. Schinckus, and H. Eugene Stanley, “Econophysics and sociophysics: Their milestones & challenges,” *Physica A* **516**, 240–253 (2019).
 - ⁸²S. Drożdż and P. Oświęcimka, “Detecting and interpreting distortions in hierarchical organization of complex time series,” *Physical Review E* **91**, 030902 (2015).
 - ⁸³S. Drożdż, R. Gębarowski, L. Minati, P. Oświęcimka, and M. Wątopek, “Bitcoin market route to maturity? Evidence from return fluctuations, temporal correlations and multiscaling effects,” *Chaos* **28**, 071101 (2018).
 - ⁸⁴J. Kwapień, M. Wątopek, M. Bezbradica, M. Crane, T. Tan Mai, and S. Drożdż, “Analysis of inter-transaction time fluctuations in the cryptocurrency market,” *Chaos* **32**, 083142 (2022).
 - ⁸⁵M. Wątopek, J. Kwapień, and S. Drożdż, “Multifractal cross-correlations of bitcoin and ether trading characteristics in the post-COVID-19 time,” *Future Internet* **14** (2022).
 - ⁸⁶X. Brouty and M. Garcin, “Fractal properties, information theory, and market efficiency,” *Chaos, Solitons & Fractals* **180**, 114543 (2024).
 - ⁸⁷K. Pearson, “Note on regression and inheritance in the case of two parents,” *Proceedings of the Royal Society of London* **58**, 240–242 (1895).
 - ⁸⁸M. L. Mehta, *Random Matrices* (Elsevier, 2004).
 - ⁸⁹J. Wishart, “The generalised product moment distribution in samples from a normal multivariate population,” *Biometrika* **20A**, 32–52 (1928).
 - ⁹⁰V. A. Marčenko and L. A. Pastur, “Distribution of eigenvalues for some sets of random matrices,” *Mathematics of the USSR-Sbornik* **1**, 457–483 (1967).
 - ⁹¹V. Plerou, P. Gopikrishnan, B. Rosenow, L. A. N. Amaral, T. Guhr, and H. E. Stanley, “Random matrix approach to cross correlations in financial data,” *Physical Review E* **65**, 066126 (2002).
 - ⁹²J. Kwapień and S. Drożdż, “Physical approach to complex systems,” *Physics Reports* **515**, 115–226 (2012).
 - ⁹³M. McDonald, O. Suleman, S. Williams, S. Howison, and N. F. Johnson, “Detecting a currency’s dominance or dependence using foreign exchange network trees,” *Physical Review E* **72** (2005).
 - ⁹⁴J. Kwapień, S. Drożdż, and P. Oświęcimka, “The bulk of the stock market correlation matrix is not pure noise,” *Physica A* **359**, 589–606 (2006).
 - ⁹⁵M. Wątopek, S. Drożdż, P. Oświęcimka, and M. Stanuszek, “Multifractal cross-correlations between the world oil and other financial markets in 2012–2017,” *Energy Economics* **81**, 874–885 (2019).
 - ⁹⁶J. Kwapień, M. Wątopek, and S. Drożdż, “Cryptocurrency market consolidation in 2020–2021,” *Entropy* **23** (2021).
 - ⁹⁷J. B. Kruskal, “On the shortest spanning subtree of a graph and the traveling salesman problem,” *Proceedings of the American Mathematical Society* **7**, 48–50 (1956).
 - ⁹⁸R. C. Prim, “Shortest connection networks and some generalizations,” *Bell System Technical Journal* **36**, 1389–1401 (1957).
 - ⁹⁹V. D. Blondel, J.-L. Guillaume, R. Lambiotte, and E. Lefebvre, “Fast unfolding of communities in large networks,” *Journal of Statistical Mechanics: Theory and Experiment* **2008**, P10008 (2008).
 - ¹⁰⁰E. Ravasz and A.-L. Barabási, “Hierarchical organization in complex networks,” *Physical Review E* **67**, 026112 (2003).